Combined Boundary-Medial Shape Description of Variable Biological Objects

by

Martin Andreas Styner

Chapter 6

Discussion and conclusions

6.1 Computation costs

The computation costs for the different algorithms were computed in several experiments with different populations of anatomical objects: single figure model for a lateral ventricle population; single figure model for a hippocampus population; four figure model for a hippocampus-amygdala complex population. The computation time depends on the processor type and the amount of available memory. The later is quite important in our computations since the methods are implemented to be computationally efficient by sacrificing memory efficiency. The values presented in Table 6.1 are computed on a processor of type SUN Ultra-Sparc II and enough memory to fit the whole process at all time. A memory size of 750 MB on a Sparc Ultra 10 station satisfies these conditions.

The tools "IRIS" and "AVS" were used for the preprocessing the data. The "param" tool developed by C. Brechbühler is used for the parameter optimization. The remaining steps of the SPHARM computation are performed using Mathematica. All other computations are performed with the "VSkelTool" program that I have developed in this dissertation. For the m-rep fitting process "VSkelTool" calls library procedures in the "pablo" tool, which is being developed within the MIDAG group at UNC.

The high cost of computing the minimal m-rep sampling can be approached by using multiple workstations. The algorithms involved in computing the sampling continuously store intermediate values to the disk. This allows the computation to be continued at the point of the last stored intermediate value if the algorithm or the computer crashes. This can happen in case of electricity failure or memory problems. Since these intermediate values can also be accessed by other "VSkelTool" processes through network transparent file systems, the computation time of the optimal m-rep sampling can be reduced linearly with the number of "VSkelTool" processes running on different machines.

	Step	Tool	Aut.	Approx. costs
A	Preprocessing of segmented object	IRIS, AVS	No	∼30 m/object
B	Parameter optimization	param	Yes	∼30 m/object
C	SPHARM description	Mathematica	Yes	∼10 m/object
D	A+B+C for population of 30 objects	-	-	∼35 h/pop.
E	Shape space and object set	Mathematica	Yes	∼30 m/pop.
F	PDM description	Mathematica	Yes	∼5 m/object
G	Inner Voronoi skeleton	VSkelTool	Yes	∼5 m/object
H	Pruned/grouped Voronoi skeleton	VSkelTool	Yes	∼40 m/object
I	Warping object set	VSkelTool	Yes	∼5 m/pop.
J	Common topology extraction	VSkelTool	Yes	∼5 m/pop.
K	E+F+G+H+I+J for 25 object set members	-	-	∼21 h/pop.
L	M-rep sampling of single sheet	VSkelTool	Yes	∼1 m/object
M	Fit of a single figure M-rep	VSkelTool	Yes	∼ 2 h/object
N	Optimal sampling for a single object	VSkelTool	Yes	∼ 90 h/pop.
O	Optimal sampling of object set	VSkelTool	Yes	∼ 300 h/pop.
P	D+K+O Total estimated time cost	-	-	∼ 350 h/pop.

Table 6.1: Estimated computation costs for all stages in the m-rep model computation scheme, measured per object or per population (pop.). The costs are computed for a single figure m-rep model. The computation time is independent of the number of figures with the exceptions of steps L, M, N and O, which are scaled linearly with the number of figures. The computation platform is a SUN Sparc Ultra 10 workstation with 750 MB of memory (i.e., large enough to fit the process)

6.2 Stability

Shape space - All computations of the common m-rep model are based on the shape space determined via PCA. In my experimants PCA has shown to be a quite stable procedure that produces good results in leave-one-out experiments (see also section A). The PCA shape space stabilizes the computation of the common m-rep model by removing shape variations due to noise. A leave-one-out analysis should be performed on the PCA with following computation of the m-rep model, which would take several weeks of computations. This has not been performed in this dissertation.

Common medial branching topology - I consider the stability of the common medial branching topology to be very good. I performed several tests that confirmed this hypothesis. The tested anatomical brain structures were the following ones: hippocampus-amygdala, hippocampus, lateral ventricles, putamen, globus pallidus and thalamus. The common branding topology depends strongly on the boundary correspondence. Although I have not experienced problems with the quality of the boundary correspondence, it is evident that for objects with a high degree of rotational symmetry the first order ellipsoid correspondence is not appropriate. In this case, the common branching topology couldn't be extracted reliably.

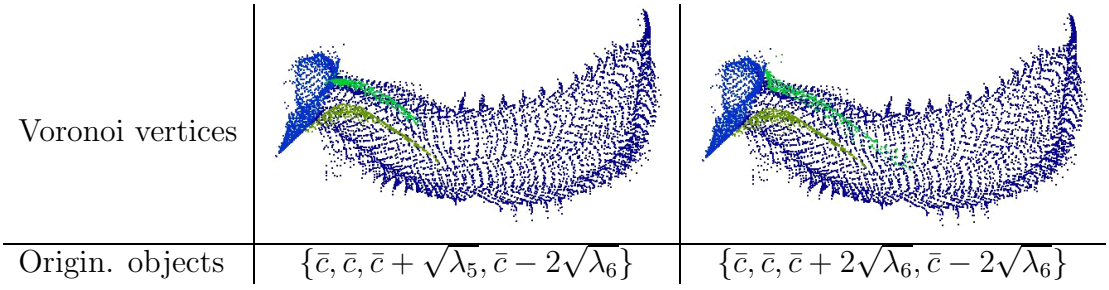

Fig. 6.1: Computed common branching topology for 2 different orderings of the matching procedure. Top row: Display of the Voronoi vertices (sheets are color coded). Bottom row: List of objects in the shape space from which the medial sheets are originating. Left: Branching topology from the implemented ordering. Right: Branching topology from a (different) random ordering. The graph properties are the same in both cases. The spatial distributions of the sheets are similar.

In my tests, the procedure has shown to be quite robust to the ordering of the object set. Changing the ordering results in the same graph properties of the branching topology. The originating objects of the medial sheets might change but the sheets and their spatial distributions remain similar. Suggested by my experiments, an ordering is likely to generate the same number of sheets and similar spatial distributions as other, different orderings (see also Fig. 6.1).

Minimal sampling computation - The borders of the Voronoi skeleton are sensitive to small perturbations on the boundary, unlike the center part of the skeleton, which is quite stable. Thus the properties of the sampled m-rep atoms are quite

stable in the grid center but not as stable at the grid edges. The computation the grid dimensions for a single population is stable. My experiments suggest that the grid dimensions for a similar population are unlikely to be the same, but they are likely to be close. Thus the grid dimension computation can be considered to be at least not unstable.

M-rep fit procedure - The m-rep fit procedure starts from an position that is close to the final position because the boundary correspondence is used to compute the initial position. The change of the m-rep properties during the fit procedure is strongly constrained by a prior on neighboring atoms. This prevents the m-rep atoms to move freely on the medial sheet if the radial function is constant along all directions. The fit procedure is non-deterministic but due to the strong prior, the stability and reliability can be considered good.

Conclusion - A quantitative analysis on the stability has not yet been performed. If the common medial model for 2 similar populations (e.g., 2 different studies of the same structure regarding the same disease) is computed, I expect to compute very similar medial branching topologies, similar grid parameters, very similar m-rep properties in the center and less similar m-rep properties at the edge of the grid. The model is constructed for a population only once, and its extraction is mainly deterministic and repeatable. Thus, in contrast to the stability of the extraction of a medial model from a single object with noise, I consider the stability of a medial model for a *single* population as stable.

6.3 Homology

The main influencing factors of establishing homologous properties for the m-rep atoms are schematically visualized in Fig. 6.2. First, the common model is highly influenced by the Voronoi skeletons and the common frame, which is based on the boundary correspondence. The warp of the common m-rep model into every individual case is purely based on the boundary correspondence. Thus, the properties of the m-rep atoms prior to the fit procedure is mainly determined by the 'warp'-influence of the boundary correspondence transferred to the Voronoi skeletons. In the m-rep fit procedure, the m-rep is adjusted to maximize a boundary match at its implied boundary while it is constrained by the initial position. A strong neighborhood dependant prior prevents the medial atoms from moving freely on the medial sheet. In summary, the established m-rep homology strongly depends on the boundary homology.

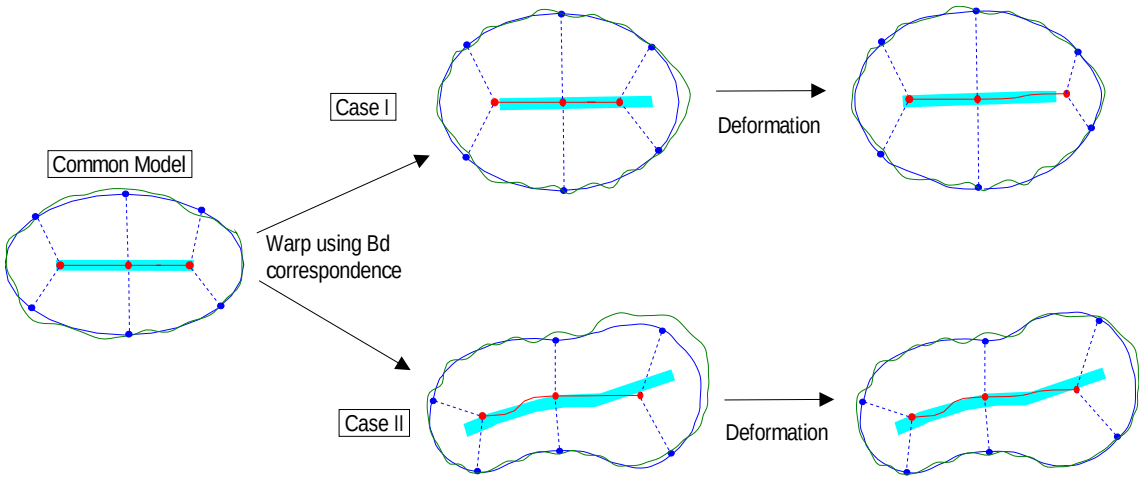

Fig. 6.2: Schematic 2D visualization of the homology for the medial description (red) and its implied boundary (blue) in two cases (I + II). The common model (left) gets warped into every individual case (middle) and then deformed into the fine scale boundary (green). The skeleton implied by the boundary is shown in cyan. The final positions of the m-rep atoms do not have to be on the skeleton since the m-rep is a coarse scale description and the skeleton is a fine scale description. The homology strongly depends on the boundary correspondence.

6.4 Conclusions

In this dissertation I presented a new approach to the description and analysis of shape in the presence of shape variability. The proposed description is based on the boundary SPHARM and the medial m-rep description. The generation of the m-rep description takes into account the shape variability of a set of training objects, which is a novel concept and a step towards a shape representation for natural objects. Using the m-rep description, locally computed shape features can quantitate and visually illustrate asymmetry or similarity. Since a correspondence is given on both the boundary and the medial manifold, a statistical analysis can directly be applied.

The SPHARM description and thus also the derived m-rep is constrained to objects of sphere topology. Also, the SPHARM boundary correspondence has shown to be a good approach in the general case, but it has inherent problems in special cases presenting rotational symmetry.

The choice of a *fixed* topology for the m-rep description has the advantages of enabling an implicit correspondence for statistical analysis. However, a fixed topology m-rep cannot precisely capture the topology of an individual object. The determined individual m-rep is therefore always an approximation, which emphasizes my decision to provide a coarse scale m-rep description.

The medial representation is constrained by the assumption that the shape variability can be captured based on the shape space spanned by the principal component analysis of SPHARM. It is thus not guaranteed that I am able to describe pathological objects not represented in the shape space. However, such pathological objects can be detected by inspecting the approximation error. Also, the m-rep model computation is designed for objects whose major deformation eigenmodes of the fine-scale boundary incorporate the coarse scale deformations. The computed m-rep model will not be appropriate if the deformation eigenmodes comprise a significant component of fine-scale deformation.

The results on the hippocampus-amygdala population in chapter 5.2 show that the choice of the training population is important. The subjects of the training population have to incorporate most of the shape variability in the desired population. If that is not the case, then the computed m-rep model will not appropriately describe the population. In the presented applications, I showed that the m-rep model computation is able to incorporate a large shape variability. Thus, an m-rep model can be computed for a population that in fact is a collection of sub-populations. For example, an m-rep model can be computed that incorporates the patient and control population instead of computing two separate m-rep models. The disadvantage of such a super-population is the increased dimensionality of the shape space because the super-population's variability is likely to increase the number of principle modes to capture 95% variability.

All parts of the presented scheme have been implemented, applied and tested. The scheme has been applied to populations of several structures of neurological interest: hippocampus-amygdala(60 cases), hippocampus(20), thalamus(56), globus pallidus(56), putamen(56) and lateral ventricles(40). However, I expect that highly

complex objects like the cortex of a human brain would be hard to handle without further adaption of the algorithms.

6.4.1 Scientific contributions of this dissertation

This section shortly summarizes the new developments and findings that this dissertation could contributed to different fields of this multi-disciplinary research project.

1. I have developed new shape description scheme that incorporates prior statistical knowledge about the shape variability. The scheme is presented in chapter 3, and the methods are described in chapter 4. The shape description scheme is suitable for shape analysis as demonstrated in the presented applications in chapter 5.

2. This work is the first to *compute* a common medial branching topology for a population of objects. This common medial branching is necessary to deal with one of the major disadvantages of medial descriptions: the sensitivity of the branching topology to even small shape variations. In section section 4.3 the methods for the branching topology computation are presented, and the complexity of the common branching topology is shown to be of the same magnitude as the individual branching topology. The computation of the common branching topology is shown in section 6.2 to be stable.

3. In regard to computational geometry issues of Voronoi skeletons, this dissertation presents in sections 4.3.1.3 - 4.3.1.7 a novel scheme that automatically prunes 3D skeletons with results superior to those published elsewhere. My experiments showed that only a very small number of skeletal sheets are necessary to describe even quite complex objects, a surprising and encouraging finding.

4. Medial representations are known to be sensitive to small boundary perturbations. This work presents in section 4.4 a medial sampling technique that together with the m-rep fit procedure allows dealing with this sensitivity as discussed in section 6.2.

5. I presented a new shape description scheme for shape analysis via incorporating prior knowledge about the shape variability. This description scheme allows new insights and paths of exploration in various fields of morphological research as demonstrated by the applications in chapter 5. The shape features thereby are meaningful and allow to answer questions that could not be answered before.

6. I have shown an example in which shape information carries information that is superior to volume measurements. This example, which is presented in section 5.3, showed that the lateral ventricles of monozygotic twins are significantly more similarly shaped than those of dizygotic twins. I was able to describe and measure the shape similarity. Further, I was even able to describe locality and type of the shape differences, features not accessible previously.

6.5 Future work

More validation - Although the scheme has been tested on a large set of images, more validation of the scheme needs to be done. A possible validation would have to include synthetic data of two or more populations that can be separated with respect to a local effect of variable size. Also, real datasets can further be used for validation. For example, the left and right hippocampus-amygdala populations, presented in section 5.2, can be used to build one joint population and compare the m-rep model of the joint model to the individual models.

More applications - The first application presented in section 5.1 can be extended to include not only two single subjects but rather the whole set of hippocampi in this schizophrenia study. The full dataset includes 82 datasets of which 26 are controls, 28 are treatment responsive patients and 28 are treatment non-responsive patients. The m-rep model should be build on the joint population of all 82 subjects. The computed individual m-rep descriptions can be used for shape analysis to investigate the differences in the three populations.

In the second application chapter 5.2 further analysis can be done on the hippocampus-amygdala objects. An earlier analysis showed a significant difference between schizophrenia patients and controls in regard to the asymmetry index $|L - R|/(L + R)$. This difference was detected in both the volume measurements and the SPHARM $\sqrt{\text{MSD}}$ measure. Using the individual m-rep descriptions, we could investigate the locations of most significant differences.

Better statistical features - It is evident that the statistical analysis that was presented in the application chapters can be considerably improved. Instead of using the raw m-rep properties, a set of new features can be computed that separate uniform/non-uniform growth from twisting and bending. This has been proposed by Yushkevich [79] on 2D m-reps. He also introduces methods of doing a local PCA do detect locations that mostly discriminate 2 populations. The extension of these methods to 3D m-reps is probably the most important future work.

Statistical m-rep model - The computed m-rep models incorporates shape variability in the common branching topology and the medial grid dimensions. This is not the case for the medial atom properties, which are determined from the average object. The m-rep description of the individual objects could be improved if the atom properties would additionally incorporate shape variability. This would lead to a fully statistical m-rep model. Since the m-rep model has been fitted to all object set members in the shape space, a distribution for the medial atom properties is directly accessible.

Appendix A

Properties of the Principal Component Analysis (PCA)

Principal component analysis (PCA) is a rotation of the basis of a distribution. The rotation is such that the variability is concentrated in a small subset of the basis. This has 2 main effects. First, the basis directions are decorrelated given that the samples are from a single Gaussian population. Secondly, the distribution basis can be reduced by removing directions of small variability contribution.

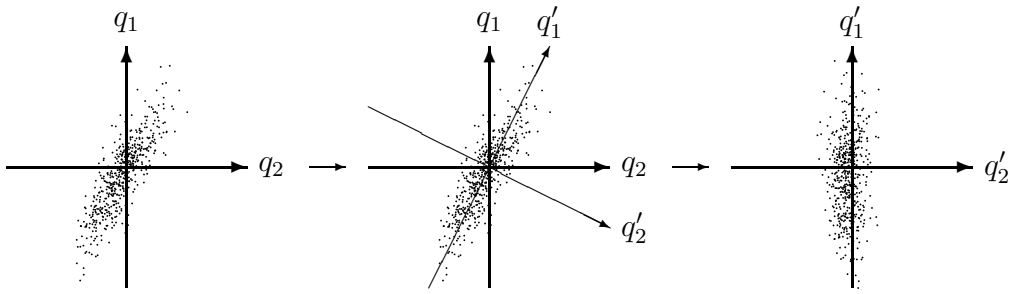

Fig. A.1: Principal component analysis as basis rotation. q_1, q_2 is the original basis, and q_1', q_2' the rotated basis after decorrelation with PCA. Clearly a decorrelation is visible as well as an ordering of the basis directions by variability contribution.

Fig. A.1 shows the PCA principle for a two-dimensional example of a Gaussian distribution. Obviously the axes q_1 and q_2 are correlated. PCA computes the new decorrelated axes q_1' and q_2', which are orthogonal linear combinations of q_1 and q_2. As much variability as possible is thereby represented in q_1'. The data could be approximated by only regarding the q_1' axis and thus reducing the dimensionality.

The principal components are computed from the empirical covariance matrix $\boldsymbol{S}$

of the training set, which is defined as

$$\boldsymbol{S} = \frac{1}{N-1} \sum_{i=1}^{N} d\mathbf{x}_i d\mathbf{x}_i^T, \tag{A.1}$$

where $d\mathbf{x}_i = \mathbf{x}_i - \bar{\mathbf{x}}$ is the deviation of the L-dimensional sample $\mathbf{x}_i$ from the arithmetic mean $\bar{\mathbf{x}} = \sum_{i=1}^{N} \mathbf{x_i}$.

The modes of variation $\mathbf{p_k}$, $k = 1 \ldots \min(L, N)$ are the unit eigenvectors of the matrix $\boldsymbol{S}$ and defined by

$$\boldsymbol{S}\, \mathbf{p}_k = \lambda_k\, \mathbf{p}_k \tag{A.2}$$

and

$$\mathbf{p}_k^T\, \mathbf{p}_k = 1, \tag{A.3}$$

where the λ_k are the eigenvalues of the matrix $\boldsymbol{S}$ ordered so that $\lambda_k \geq \lambda_{k+1}$. Rewriting equation (A.2) to

$$(\boldsymbol{S} - \lambda_k \boldsymbol{I})\ \mathbf{p}_k = 0\ , \tag{A.4}$$

where $\boldsymbol{I}$ is the identity matrix, makes clear that a set of linear equations has to be solved. Note that the number of eigenmodes of a matrix is equal to its rank. Accordingly, $\boldsymbol{S}$ has $\min(L, N)$ eigenmodes. The variance described by an eigenvector $\mathbf{p}_k$ is equal to the corresponding eigenvalue λ_k. So the eigenvectors belonging to the largest eigenvalues describe the most significant modes of variability.

In shape analysis applications, the number of samples N is often smaller than the number of parameters L gathered in the parameter vectors $\mathbf{x}_i$. The eigenmodes of the empirical covariance matrix $\boldsymbol{S} = \frac{1}{N-1} \sum_{i=1}^{N} d\mathbf{x}_i d\mathbf{x}_i^T = \Delta\boldsymbol{X} \Delta\boldsymbol{X}^T$ can be obtained by solving for the Eigenmodes of a reduced covariance matrix. As the mean was subtracted from the $\mathbf{x}_i$, the matrix $\boldsymbol{S}$ has at most rank $N-1$ and a maximum of $N-1$ non-zero eigenvectors results from the PCA.

As a first step, one of the vectors in $\Delta\boldsymbol{X}$ is dropped so that the remaining are linearly independent. Then, an orthonormal basis $\boldsymbol{M}$ of $\Delta\boldsymbol{X}$ is obtained by applying a Gram-Schmidt procedure that takes an arbitrary basis and generates an orthonormal one.

A reduced covariance matrix $\boldsymbol{s}$ is then given by

$$\boldsymbol{s} = \frac{1}{N-1} \boldsymbol{M}^T \Delta\boldsymbol{X}\ \Delta\boldsymbol{X}^T \boldsymbol{M} = \frac{1}{N-1} \boldsymbol{M}^T \boldsymbol{S}\, \boldsymbol{M}\ . \tag{A.5}$$

Solving the reduced eigensystem for each eigenvector $\mathbf{p}_{\boldsymbol{s}i}$,

$$\boldsymbol{s}\, \mathbf{p}_{\boldsymbol{s}i} = \lambda\, \mathbf{p}_{\boldsymbol{s}i}, \tag{A.6}$$

the $(N-1)$-dimensional $\mathbf{p}_{\boldsymbol{s}i}$ yield the L-dimensional eigenvectors through

$$\mathbf{p}_i = \boldsymbol{M}\mathbf{p}_{\boldsymbol{s}i}, \tag{A.7}$$

which are gathered in the eigenvector matrix $\boldsymbol{P} = (\mathbf{p}_1, \mathbf{p}_2, \ldots, \mathbf{p}_{N-1})$.

Most of the variation can usually be explained by a relatively small number of eigenmodes t. When the number of training samples N is smaller than the number of parameters, then all variation in the training set can be described by $t = N-1$ eigenmodes. Considering a smaller number t of eigenmodes, they describe a proportion λ_t of the total variance of all variables

$$\lambda_t = \sum_{k=1}^{t} \lambda_k \; . \tag{A.8}$$

The number t of selected eigenmodes is thereby chosen considering the overall proportion of variance reflected in the selected eigenmodes or by selecting eigenmodes with eigenvalues above a given minimum. Having chosen t, any object in the training set can be approximated by a weighted sum of the first t eigenmodes and the mean object $\bar{\mathbf{x}}$.

$$\mathbf{x} = \bar{\mathbf{x}} + \boldsymbol{P}_t\mathbf{b}_t \, , \tag{A.9}$$

where $\mathbf{b}_t = (b_1, b_2, \ldots, b_{t-1}, b_t)^T$ is the weight vector, and $\boldsymbol{P}_t = (\mathbf{p}_1 \ldots \mathbf{p}_t)$ is the eigenvector matrix.

Bibliography

[1] N. Amenta, B. Marshall, and Kamvysselis M. A new voronoi-based surface recostruction algorithm. In *SIGGRAPH 1998, Computer Graphics Proceedings*, pages 415–421, 1998.

[2] N.C. Andreasen, L. Flashmann, M. Flaum, S. Arndt, V. Swayze Il, D. O'Leary, J.C. Ehrhardt, and W.T.C. Yuh. Regional Brain Abnormalities in Schizophrenia Measured with Magnetic Resonance Imaging. *JAMA*, 272(22):1763–1792, December 1994.

[3] D. Attali, G. Sanniti di Baja, and E. Thiel. Skeleton simplification through non significant branch removal. *Image Processing and Communications*, 3(3-4):63–72, 1997.

[4] Dominique Attali and Annick Montanvert. Semi-continuous skeletons of 2d and 3d shapes. In *Aspects of Visual Form Processing, World Scientific*, pages 32–41, 1994.

[5] Dominique Attali and Annick Montanvert. Computing and simplifying 2d and 3d continuous skeletons. *Computer Vision and Image Understanding*, 67(3):261–273, September 1997.

[6] J. August, K. Siddiqi, and S. Zucker. Ligature instabilities in the perceptual organization of shape. In *IEEE Computer Society Conference on Computer Vision and Pattern Recognition*, 1999.

[7] J. August, A. Tannenbaum, and S. Zucker. On the evolution of the skeleton. In *International Conference on Computer Vision*, pages 315–322, 1999.

[8] R. Bajcsy and F. Solina. Three dimensional object representation revisited. *IEEE Transactions on Pattern Analysis and Machine Intelligence*, pages 231–239, 1987.

[9] Danah H. Ballard and Christopher M. Brown. *Computer Vision*. Prentice-Hall Inc., Englewood Cliffs, New Jersey, 1981.

[10] A. Bartley, D. Jones, and D. Weinberger. Genetic variability of human brain size and cortical patterns. *Brain*, 120:257–269, 1997.

[11] T.O Blum. A transformation for extracting new descriptors of shape. In *Models for the Perception of Speech and Visual Form*. MIT Press, 1967.

[12] J.D. Boissonat and P. Kofakis. Use of the delaunay triangulation for the identification and the localization of objects. In *IEEE Computer Society Conference on Computer Vision and Pattern Recognition*, pages 398–401, 1985.

[13] F.L. Bookstein. Principal warps: Thin-plate splines and the decomposition of deformations. *IEEE Transactions on Pattern Analysis and Machine Intelligence*, 1(6), June 1989.

[14] F.L. Bookstein. *Morphometric Tools for Landmark Data: Geometry and Biology*. Cambridhe University Press, 1991.

[15] F.L. Bookstein. How to produce a landmark point: the statistical geometry of incompletely registered images. In *SPIE*, volume 2573, 1995.

[16] F.L. Bookstein. Landmark methods for forms without landmarks: Localizing group differences in outline shape. In *Workshop on Mathematical Methods in Biomedical Image Analysis*, 1996.

[17] F.L. Bookstein. Shape and the information in medical images: A decade of the morphometric synthesis. In *Workshop on Mathematical Methods in Biomedical Image Analysis*, 1996.

[18] G. Borgefors, I. Ragnemalm, and G. di. The euclidean distance transform: Finding the local maxima and reconstructingthe shape. In *SCIA Conf*, pages 974–981, 1991.

[19] J.W. Brandt and V.R. Algazi. Continous skeleton computation by voronoi diagram. *Computer Vision, Graphics, and Image Processing: Image Understanding*, 55(3):329–338, 1992.

[20] C. Brechbühler. *Description and Analysis of 3-D Shapes by Parametrization of Closed Surfaces*. Hartung Gorre, 1995. Dissertation, IKT/BIWI, ETH Zürich, ISBN 3-89649-007-9.

[21] C. Brechbühler, G. Gerig, and O. Kübler. Parametrization of closed surfaces for 3-D shape description. *CVGIP: Image Understanding*, 61:154–170, 1995.

[22] C.A. Burbeck, S.M Pizer, B.S. Morse, D. Ariely, G. Zauberman, and J Rolland. Linking object boundaries at scale: a common mechanism for size and shape judgements. *Vision Research*, 36:361–372, 1996.

[23] A. Caunce and C.J. Taylor. 3D Point Distribution Models of the Cortical Sulci. In *Sixth International Proceedings on Computer Vision*, pages 402–407, Bombay, India, January 1998. IEEE, Narosa Publishing House.

[24] G.E. Christensen, R.D. Rabbitt, and M.I. Miller. 3d brain mapping using a deformable neuroanatomy. *Physics in Medicine and Biology*, 39:209–618, 1994.

[25] T. Cootes, C. Beeston, G.J. Edwards, and C.J. Taylor. A unified framework for atlas matching using active appearance models. In *Proc. of Information Processing in Medical Imaging, IPMI'99*, pages 322–333, 1999.

[26] T.F. Cootes and C.J. Taylor. Active Shape Models - 'Smart Snakes'. In *British Mach. Vision Conf.*, pages 266–275. Springer-Verlag, 1992.

[27] JG Csernansky, S Joshi, LE Wang, J Haller, M Gado, JP Miller, U Grenander, and MI Miller. Hippocampal morphometry in schizophrenia via high dimensional brain mapping. *Proc. Natl. Acad. Sci. USA*, 95:11406–11411, September 1998.

[28] C. Davatzikos, M. Vaillant, S. Resnick, J.L Prince, S. Letovsky, and R.N. Bryan. A computerized method for morphological analysis of the corpus callosum. *J. of Comp. Ass. Tomography.*, 20:88–97, Jan./Feb 1996.

[29] Christos Davatzikos. Spatial transformation and registration of brain images using elastically deformable models. *Computer Vision and Image Understanding: CVIU*, 66(2):207–222, 1997.

[30] H. Delingette. General Object Reconstruction based on Simplex Meshes. Technical Report 3111, INRIA, 1997.

[31] L DeLisi, T William, X. Shu-hong, A. Hoff, M Sakuma, M. Kushner, G. Lee, K. Shedlack, A. Smith, and R. Grimson. A prospecrive follow-up study of brain morphology and cognition in first episode schizophrnic patients: Preliminary findings. *Biological Psychiatry*, 38:349–360, 1995.

[32] I. Dryden. Highly resistant shape analysis. Technical report, Dep. Statistics, Univ. of Chicago, June 1997.

[33] T. Fletcher, S. Pizer, A. Thall, and G Gash. Shape modeling and image visualization in 3d with m-rep object models. Technical report, Dept. of Computer Science, UNC Chapel Hill, 2000.

[34] K. Fu and Y. Tsao. A parallel thinning algorithm for 3-d pictures. *Computer Graphics and Image Processing*, 17:315–331, 1981.

[35] Y. Ge, C. Maurer, and J. Fitzpatrick. "image registration using the iterative closest point algorithm with a closestpoint transform. In *SPIE*.

[36] Peter Giblin and Benjamin Kimia. A formal classification of 3d medial axis points and their local geometry. In *IEEE Computer Society Conference on Computer Vision and Pattern Recognition*, pages 566–573, 2000.

[37] P. Golland and W.E.L. Grimson. Fixed topology skeletons. In *International Conference on Computer Vision*, 1999.

[38] P. Golland, W.E.L. Grimson, and R. Kikinis. Statistical shape analysis using fixed topology skeletons: Corpus callosum study. In *International Conference on Information Processing in Medical Imaging*, LNCS 1613, pages 382–388. Springer Verlag, 1999.

[39] R.M. Haralick. Image analysis using mathematical morphology. *IEEE Transactions on Pattern Analysis and Machine Intelligence*, 9(4):532–550, 1987.

[40] S. Joshi, M Miller, and U. Grenander. On the geometry and shape of brain submanifolds. *Pattern Recognition and Artificial Intelligence*, 11:1317–1343, 1997.

[41] S. Joshi, S. Pizer, T. Fletcher, A. Thall, and G. Tracton. Multi-scale deformable model segmentation based on medial description. In *International Conference on Information Processing in Medical Imaging*, 2001. accepted for publication.

[42] András Kelemen, Gábor Székely, and Guido Gerig. Elastic model-based segmentation of 3d neuroradiological data sets. *IEEE Transactions on Medical Imaging*, 18:828–839, October 1999.

[43] B. Kimia, A. Tannenbaum, and S. Zucker. Shape, shocks, and deformations i: The components of two-dimensional shape and the reaction-diffusion space. *International Journal of Computer Vision*, 15:189–224, 1995.

[44] Aaron Kotcheff and Chris Taylor. Automatic construction of eigenshape models by genetic algorithm. In *International Conference on Information Processing in Medical Imaging*, pages 1–14, 1997.

[45] L. Lam, S. Lee, and C. Suen. Thinning methodologies: A comprehensive survey. *IEEE Transactions on Pattern Analysis and Machine Intelligence*, 14:869–885, 1992.

[46] S. Loncaric. A survey of shape analysis techniques. *Pattern Recognition*, 31(8):983–1001, 1998.

[47] Stephane G. Mallat. A theory for multiresolution signal decomposition: The wavelet representation. *IEEE Transactions on Pattern Analysis and Machine Intelligence*, 11(7):674–693, 1989.

[48] R. McCarley, C. Wible, M. Frumin, Y. Hirayasu, J. Levitt, I. Fischer, and M. Shenton. Mri anatomy of schizophrenia. *Biological psychiatry*, 1999.

[49] M. Miller. Algorithms and codes for refining and linking of brain data. *EnVision*, 15(3):4–5, July-September 1999.

[50] M. Miller. *Brain Warping*, chapter Large deformation fluid diffeomorphisms for landmark and image matching, pages 115–131. Academic Press, 1999.

[51] M. Näf. *Voronoi Skeletons: a semicontinous implementation of the 'Symmetric Axis Transform' in 3D space*. PhD thesis, ETH Zürich, Commmunication Technology Institue, Image Analysis Group IKT/BIWI, 1996.

[52] A Pitiot, PM Thompson, and AW Toga. Spatially and temporally adaptive elastic template matching. *IEEE Transactions on Pattern Analysis and Machine Intelligence*, 1999.

[53] S. Pizer, D. Fritsch, P. Yushkevich, V. Johnson, and E. Chaney. Segmentation, registration, and measurement of shape variation via image object shape. *IEEE Transactions on Medical Imaging*, 18:851–865, October 1999.

[54] William H. Press, Saul A. Teukolsky, William T. Vetterling, and Brian P. Flannery. *Numerical Recipes in C*. Cambridge Univ. Press, 2 edition, 1993. `http://www.ulib.org/webRoot/Books/Numerical_Recipes/bookcpdf.html`.

[55] A. Rangarajan, H. Chui, and F. Bookstein. The softassign procrustes matching algorithm. In *International Conference on Information Processing in Medical Imaging*, number 1230 in LNCS, pages 29–42, 1997.

[56] M. Schmitt. *LNCS:Geometry amd robotics*, volume 391, chapter Some Examples of Algorithms Analysis in Computational Geometry by Means of Mathematical Morphological Techniques, pages 225–246. Springer Verlag, 1989.

[57] M.E. Shenton, C.G. Wible, and RW McCarley. *Brain Imaging in Clinical Psychiatry*, chapter MRI studies in schizophrenia, pages 297–380. Marcel Decker Inc., 1997.

[58] F. Y. Shih and C. C. Pu. A skeletonization algorithm by maxima tracking on Euclidean distance transform. *Pattern Recognition*, 28(3):331–341, 1995.

[59] K. Siddiqi, A. Ahokoufandeh, S. Dickinson, and S. Zucker. Shock graphs and shape matching. In *International Conference on Computer Vision*, January 1998.

[60] K. Siddiqi, A. Ahokoufandeh, S. Dickinson, and S. Zucker. Shock graphs and shape matching. *International Journal of Computer Vision*, 1(35):13–32, 1999.

[61] K. Siddiqi, S. Bouix, A. Tannenbaum, and S. Zucker. The hamilton-jacobi skeleton. In *International Conference on Computer Vision*, 1999.

[62] K. Siddiqi, B. Kimia, S. Zucker, and A. Tannenbaum. Shape, shocks and wiggles. *Image and Vision Computing Journal*, 17:365–373, 1999.

[63] K. Siddiqi, A. Tannenbaum, and S. Zucker. Hyperbolic smoothing of shapes. In *International Conference on Computer Vision*, 1998.

[64] R. Sprengel, K. Rohr, and H. Stiehl. Thin-plate spline approximation for image registration. In *Internat. Conf. of the IEEE Engineering in Medicine and Biology Society*, 1996.

[65] L.H. Staib and J.S. Duncan. Boundary Finding with Parametrically Deformable Models. *IEEE Transactions on Pattern Analysis and Machine Intelligece*, 14(11):1061–1075, November 1992.

[66] L.H. Staib and J.S. Duncan. Model-based Deformable Surface Finding for Medical Images. *IEEE Trans. Med. Imaging*, 15(5):1–12, 1996.

[67] M. Styner and G. Gerig. Evaluation of 2d/3d bias correction with 1+1es-optimization. Technical Report 179, Image Science Lab, ETH Zürich, 1997.

[68] M Styner and G. Gerig. Hybrid boundary-medial shape description for biologically variable shapes. In *Proc. of IEEE Workshop on Mathematical Methods in Biomedical Image Analysis (MMBIA) 2000*, pages 235–242, June 2000.

[69] M Styner and G. Gerig. Medial models incorporating shape variability. In *International Conference on Information Processing in Medical Imaging*, 2001. accepted for publication.

[70] G Subsol, J.P. Thirion, and N. Ayache. A scheme for automatically building three-dimensional morphometric anatomical atlases: application to a skull atla. *Medical Image Analysis*, 2(1):37–60, 1998.

[71] G. Székely. Shape characterization by local symmetries, 1998. Habilitation, ETH Zürich.

[72] G. Székely, A. Kelemen, Ch. Brechbühler, and G. Gerig. Segmentation of 2-D and 3-D objects from MRI volume data using constrained elastic deformations of flexible Fourier contour and surface models. *Medical Image Analysis*, 1(1):19–34, 1996.

[73] H. Tagare. Non-rigid curve correspondence for estimating heart motion. In *International Conference on Information Processing in Medical Imaging*, pages 489–494, 1997.

[74] H. Tagare, D. O'Shea, and A. Rangarajan. A geometric criterion for shape-based non-rigid correspondence. In *International Conference on Computer Vision*, pages 434–439, 1995.

[75] Hüseyin Tek and Benjamin Kimia. Curve evolution, wave propagation, and mathematical morphology. In *International Conference on Computer Vision*, June 1998.

[76] Hüseyin Tek and Benjamin Kimia. Symmetry maps of free-form curve segments via wave propagation. In *International Conference on Computer Vision*, 1999.

[77] D'Arcy Thomson. *On Growth and Form*. Cambridge University Press, second edition, 1942.

[78] AW Toga. *Brain warping*. Academic Press, 1999.

[79] P. Yushkevich and S. Pizer. Coarse to fine shape analysis via medial models. In *International Conference on Information Processing in Medical Imaging*, 2001. accepted for publication.